Supporting Information

Graphene and hydroxyapatite self-assemble into homogenous, free standing nanocomposite hydrogels for bone tissue engineering

Xingyi Xie,[a,b,‡] Kaiwen Hu,[b,‡] Dongdong Fang,[c] Lihong Shang,[b] Simon D. Tran [c] and Marta Cerruti *[,b]

[a] College of Polymer Science and Engineering, State Key Laboratory of Polymer Materials and Engineering, Sichuan University, Chengdu, Sichuan, 610065, China.

[b] Department of Mining and Materials Engineering, McGill University, Montreal, QC, H3A 0C5, Canada.

[c] Craniofacial Tissue Engineering, Faculty of Dentistry, McGill University, Montreal, QC, H3A 0C7, Canada

[‡] These authors equally contributed to the paper.

*Corresponding author; e-mail: marta.cerruti@mcgill.ca. Tel: 1-514-3985496; Fax: 1-514-3984492

Experimental Section

Characterizations

The rGO and G/HA hydrogels were freeze dried at −100 °C and 20 mT for 2 d (BT4KZL VirTis benchtop freeze-dryer, Boston Laboratory Equipment, Woburn, MA, USA) and then subjected to various structural characterizations. The solid content was calculated based on the weight change before and after freeze drying. The crystalline phases were identified by XRD analysis using a D8 Discovery instrument (Bruker-AXS Inc, Madison, Wisconsin, USA) equipped with Vantec 2000 area detector and Cu Kα X-ray source (λ=1.54056Å). A step size of 0.005° of 2θ was used and the spacing of lattice planes was calculated according to Bragg's law as $d=\lambda/(2\mathrm{Sin}\theta)$. The elemental composition was analyzed by XPS on a Thermo Scientific K-Alpha photoelectron spectrometer (Thermo Fisher Scientific Inc., Waltham, Massachusetts, USA).Three spots with 400 μm in diameter were randomly selected for each analyzed surface or section. Three survey scans in the range of 0–1350 eV with a step size of 1 eV were collected to determine elemental species and their atomic contents. High resolution scans with a step size of 0.1 eV were repeated at least 5 times for each detectable element. C_{1S} spectra were

curve-fitted with four components,[1,2] with C−C(C=C), C−O(C−N), C=O, O−C=O at 284.8, 286.3, 288.1 and 289.2 eV, respectively. Depth profiles were performed in-situ using an Ar ion beam sputtering, with energy of 3000 eV, at "middle" current level as specified in the software. The same etching conditions provide an etching rate of 0.72 nm s^{-1} on Ta_2O_5. Each etching cycle lasted 20 s. ATR-FTIR spectra were recorded on a Spectrum-Two IR spectrometer (Perkin Elmer, Waltham, Massachusetts, USA) with the accumulation of 32 scans in the range of 400–4000 cm^{-1} at a resolution of 4 cm^{-1}. Raman spectra were obtained on a Bruker Senterra confocal Raman microscope and spectrometer (Bruker Optics Inc., Massachusetts, USA) using a laser at 532 nm with 5 mW power. HA content were measured by TGA on a Q500 thermogravimetric analyzer (TA Instruments, USA) in air, using a ramp from RT to 900 °C with a heating rate of 20 °C min^{-1}. The N_2 adsorption/desorption isotherms at 77K were measured on a Micrometric TriStar Surface area and porosity analyzer (Micromeritics Instrument Corporation, Norcross, Georgia, USA).

The morphology was observed under an Inspect 50 SEM (FEI, Tokyo, Japan) operated at 5 kV with spot size 2. Energy dispersive X-ray spectroscopy was also performed on this machine operated at 10 kV with spot size 3. High resolution morphology and lattice structures were observed under a CM200 TEM (Philips, Amsterdam, Netherlands) operated at 200 kV.

Mechanical properties of the hydrogel samples were measured on a Mach-1 mechanical tester (Biomomentum Inc., Laval, Quebec, Canada) in a compression setup. A crosshead speed of 0.03 mm s^{-1} was used, approximating the strain rate of 10% per min recommended in ASIM 1621. Current–voltage (*I*–*V*) sweeping was performed for two times from −10 mV to +10 mV on both ends of each cylindrical hydrogel, using a B1500A semiconductor devices analyzer (Agilent Technologies Inc., California, USA). The perfect match of both sweepings suggested the stable electric conduction of the sample. The slope of each *I*–*V* curve represents the conductance (*G*). The conductivity (κ) was calculated as $\kappa=4LG/\pi D^2$, where *L* and *D* are the length and diameter of the test hydrogel.

Isolation of mouse multipotent mesenchymal stromal cells (MSCs)

Mouse MSCs were harvested as described previously.[3] Briefly, 8-week old male C3H mice were sacrificed. Tibias and femurs were dissected and muscles were removed thoroughly. Bones were crushed gently in 10 mL phosphate buffered saline (PBS) containing 2% fetal bovine serum and 1mM EDTA. Bone marrow was flushed away and cells were cultured in the mouse stem cell medium of MesenCult™ Proliferation Kit with MesenPure™ (Catalog No. 05512, Stem Cell Technologies, Vancouver, BC, Canada). Compact bones were digested in 0.25%

Collagenase Type I in PBS containing 20% fetal bovine serum for 45 min. Suspension was strained through a 70 μm cell strainer, followed by centrifugation at 300 *g* at room temperature for 10 minutes. The cells were cultured in 100-mm dish containing the MesenCult™ Proliferation Kit medium (Catalog No. 05511, Stem Cell Technologies). After two passages, both bone marrow cells and compact bone cells were harvested. Unwanted hematopoietic cells were labeled with magnetic particles by using antibodies against CD45/TER119 expressed on the membranes of these cells, then were separated from unlabeled targeting cells using a magnet. The resulting $CD45^-/TER119^-$ cells were cultured for one to two passages. These cells have been tested previously to have characteristics of MSCs as they were tissue culture polystyrene (plastic) adherent, positive for Sca-1, CD106, CD105, CD73, CD29, CD44, negative for CD45, TER119, CD11b, had a high number of colony forming unit-fibroblast (CFU-F), and differentiated into osteocytes, chondrocytes and adipocytes.[3]

Cell viability and morphology

The rGO and G/HA-40 hydrogels were cut into 1-mm-thick disks, each being placed in a 24-well plate. The mouse $CD45^-/TER119^-$ MSCs were seeded onto the sample disks at 20,000 cells per well, with three replicates. Standard tissue culture polystyrene (TCP) served as control. After 2 days of culture, cells were washed with 1 mL of PBS for three times. PBS containing 2 μM Ethidium homodimer-1 and 1 μM Calcein AM were added and incubated for 10 min at 37°C to stain the dead cells and live cells, respectively. After washing three times, cells were imaged under Zeiss Axio Imager M2 microscope (Carl Zeiss Microscopy GmbH, Goettingen, Germany). Red fluorescence indicated dead cells while green, live cells. The density and percentage of live cells were counted with Image J software for at least 8 view fields per sample under 50× magnification. Each view field used for cell viability assessment was 5.83 mm^2.

For cell morphology, the cells were seeded as described above and were fixed using 2% glutaraldehyde in PBS for 2 d at 4 °C. Samples were then rinsed with distilled water and then dehydrated through graded ethanol solutions (30%, 50%, 70%, 80%, 90%, 95% and 100%) for 20 minutes in each. After drying on an Automegasamdri®-915B, Series B supercritical point dryer (Tousimis, Rockville, Maryland, USA), the samples were coated with 2-nm-thick platinum using a Leica EM ACE 600 high vacuum coater (Leica Microsystems Inc, Wetzlar, Germany) and imaged under an Inspect 50 SEM (FEI, Tokyo, Japan).

Supplementary Figures

Figure S1

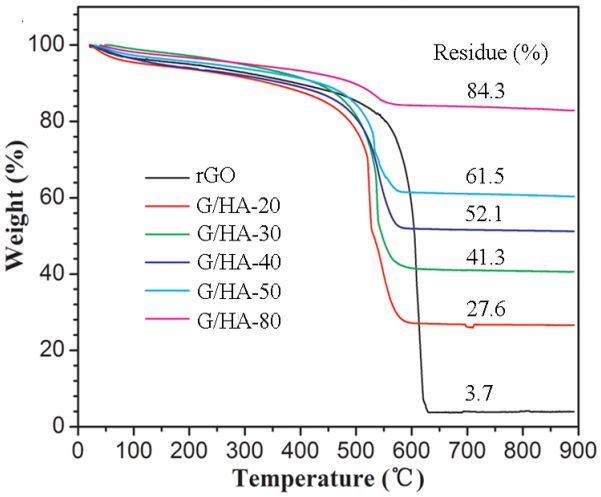

Figure S1. TGA curves showing higher HA content in each G/HA composite than the corresponding HA feed (see Table 1, main text).

All the G/HA samples have lower decomposition temperatures than rGO, suggesting the looser graphene stacking in the composites than in rGO.

Figure S2

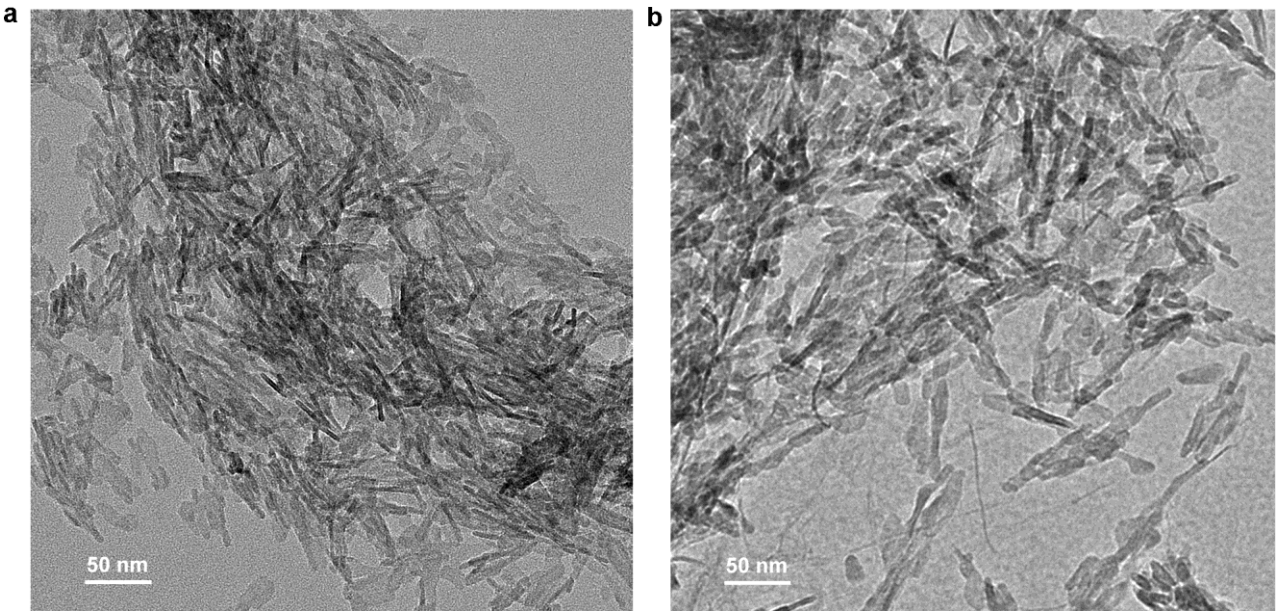

Figure S2. TEM images showing HA morphology before (a) and after (b) the hydrothermal treatment.

(**a**) TEM image of the initial HA NPs, obtained after dialysis of a solution (33.3 mg mL^{-1}) for 5 days, with 2 water exchanges per day. (**b**) TEM image of the HA NPs deposited on reduced graphene flakes, from G/HA-40. Both HA samples display rod-like morphology, but the hydrothermal treatment doubles the diameter of the HA NPs.

Figure S3

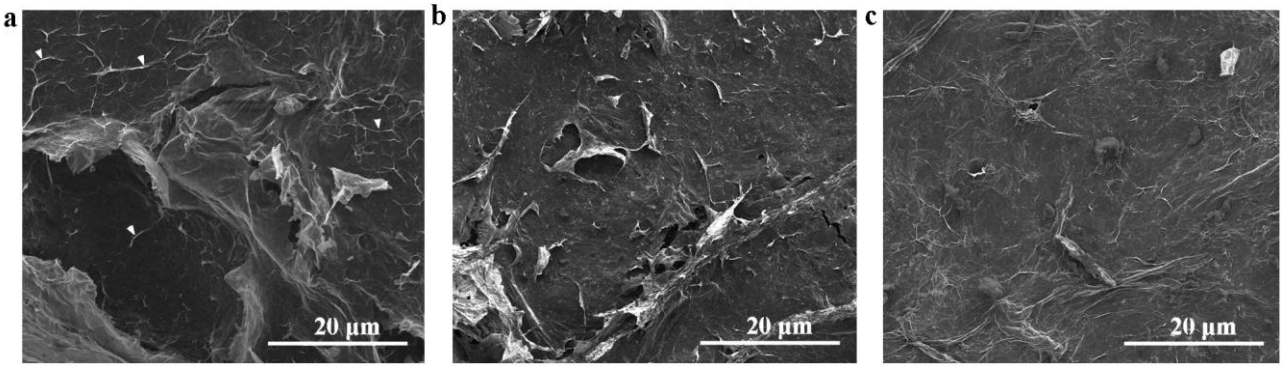

Figure S3. SEM images of the side (a), top (b) and bottom (c) shell encapsulating G/HA-20.
The side view shows some roughness due to the edges of packed graphene flakes; a few examples are indicated by arrow heads (**a**). This rough texture is hardly found on the top (**b**) and bottom (**c**) views, suggesting that the graphene flakes are packed more densely on the top and bottom shells than on the side shell.

Figure S4

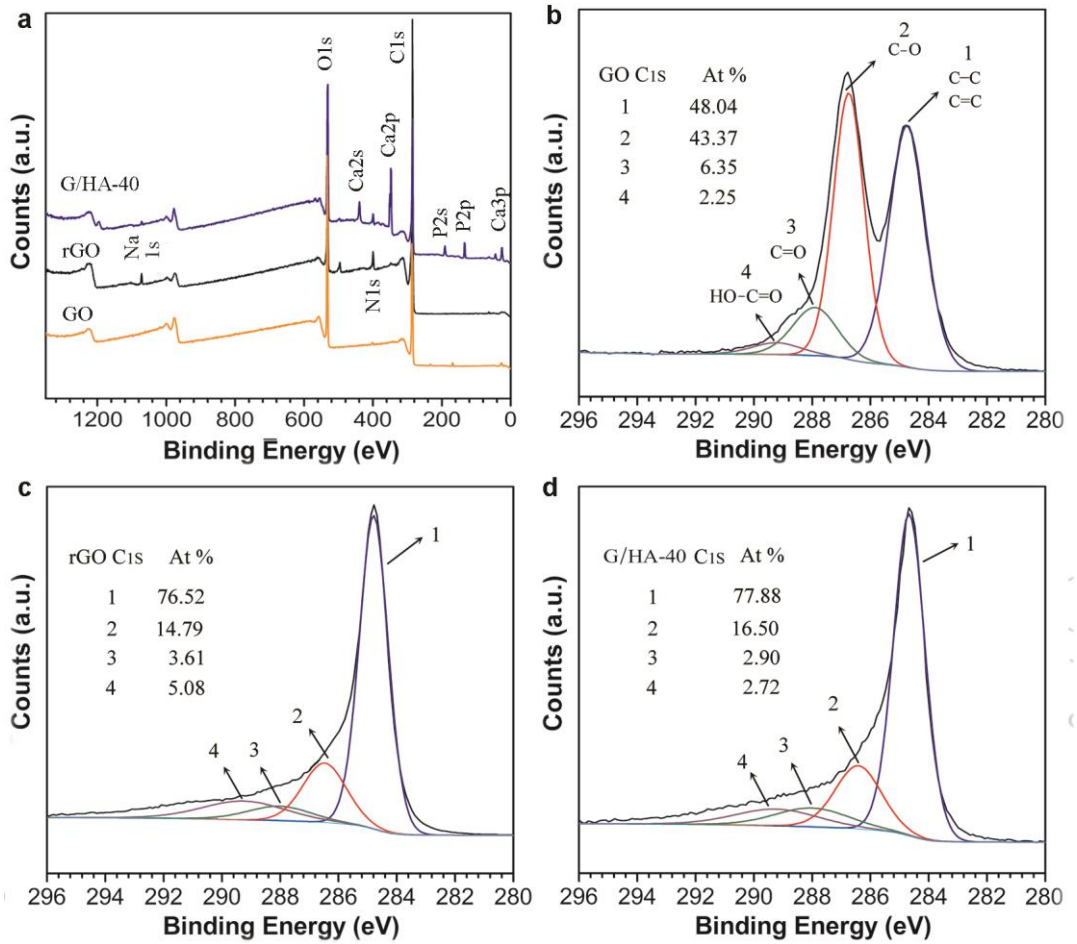

Figure S4. XPS survey (a) and high resolution C_{1s} spectra of GO (b), rGO (c) and G/HA-40 (d), measured on cross-section relative to the bulk of each sample.

The atomic % extrapolated from the survey spectra are reported in Table S1. The values reported on each high resolution spectra refer to the relative percentage of each component that we have used to deconvolute the spectra. These components are labeled 1 through 4, and are ascribed to C environments relative to C–C and C=C bonds (component 1, centered at an energy of 284.8 eV), C–O bonds (component 2, at 286.3 eV), C=O bonds (component 3, at 288.1 eV) and COOH bonds (component 4, at 289.2 eV).

Figure S5

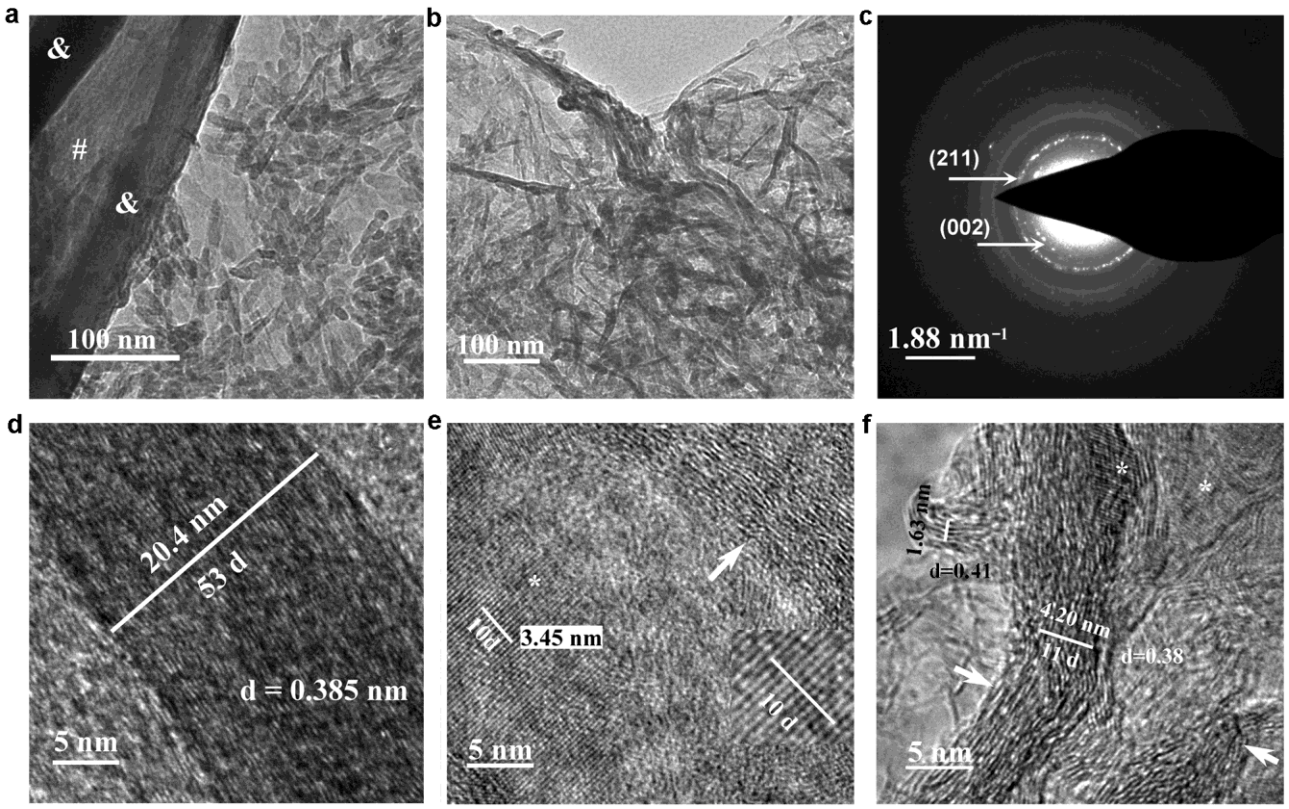

Figure S5. TEM images of G/HA-40.

(**a**) Two parallel stacks ("&" labels) in the shell sandwich an HA layer ("#" label). HA NPs clearly display their rod-shaped morphology, with size of 20–35 nm in length and 4.3–5.1 nm in diameter (n=5). (**b**) Randomly oriented HA particles attach on bulk graphene stacks. (**c**) Selected area (from **b**) electron diffraction pattern reveals d-spacings of 2.81 Å and 3.46 Å, corresponding to HA (002) and (211) lattice plane, respectively. The scale bar represents the reciprocal of interlayer spacing (d^{-1}). (**d**) An individual graphene stack from the shell possessed a d-spacing of 3.85 Å. (**e, f**) High resolution TEM images show d-spacing of 3.45 Å in HA particles (asterisks) and of 3.9±0.1 Å (n=6, also from Fig. 3f, main text) in bulk graphene stacks (white arrows).

Figure S6

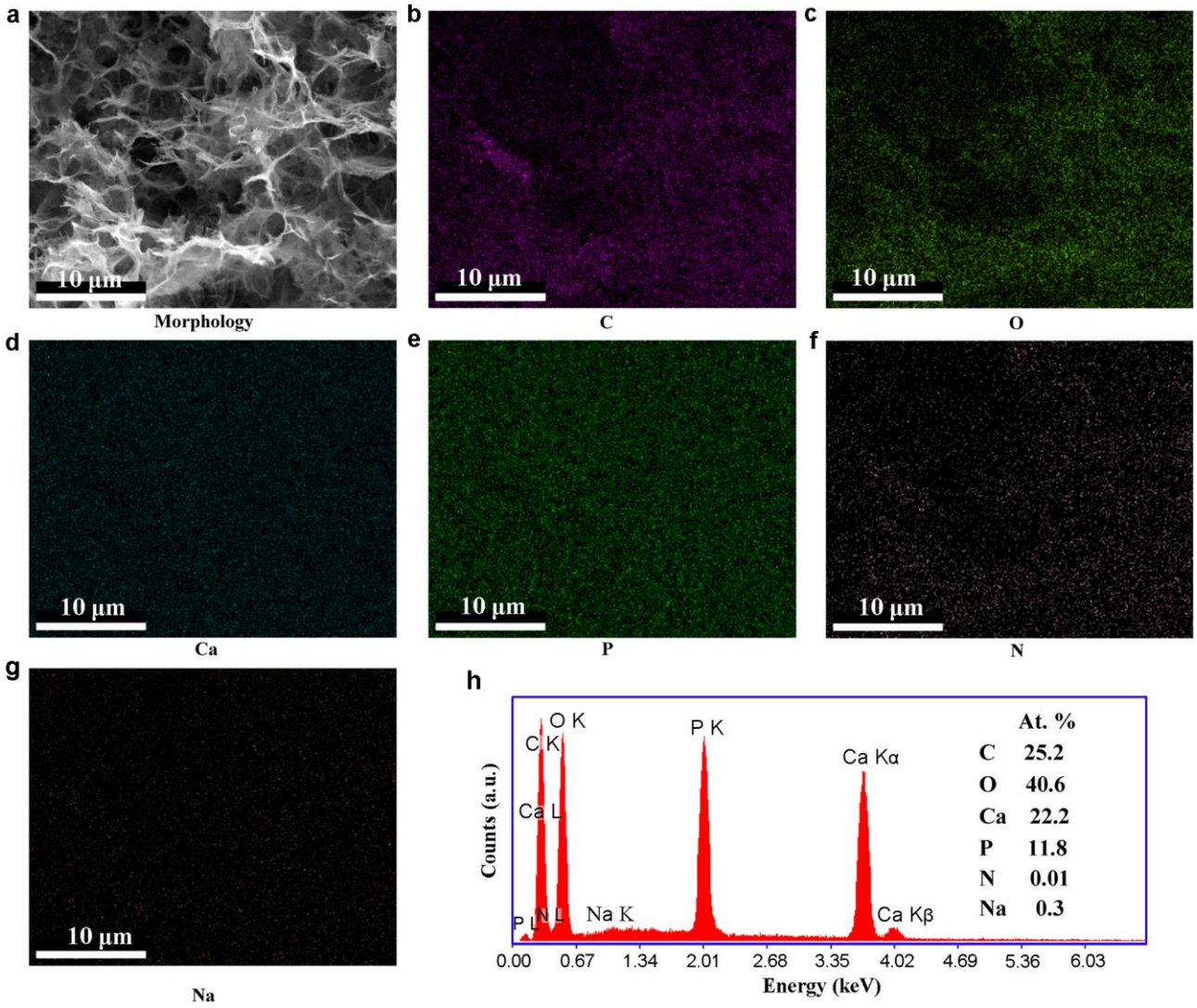

Figure S6. SEM bulk morphology (a) and EDS elemental mapping (b-g) of G/HA-40.

All the elements are uniformly distributed. Note that the semi-quantitative results (**h**) show higher Ca and P contents than those obtained from XPS. This is because the EDS detector is less sensitive to lower energy X-rays (like those emitted from C and N elements).[4]

Figure S7

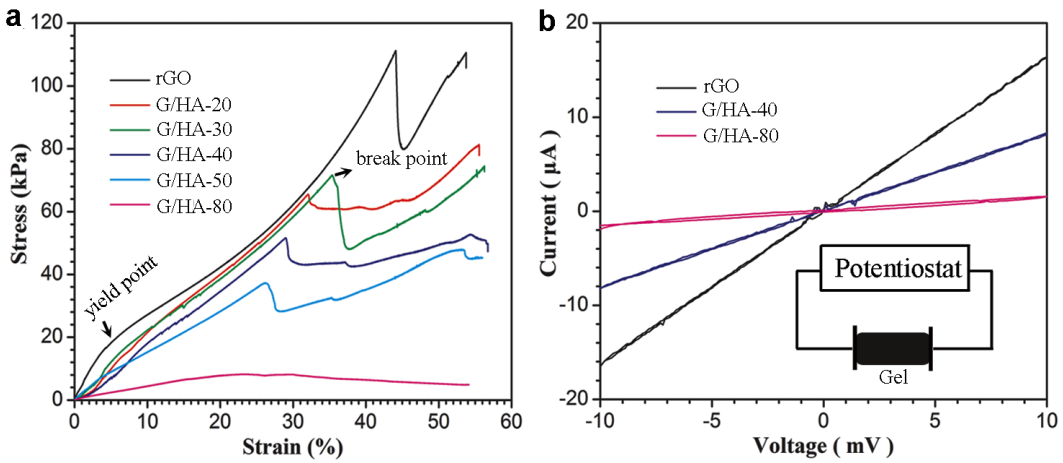

Figure S7. Mechanical and electrical properties of G/HA composites.

(**a**) Typical stress-strain curves reveal a general decrease in mechanical properties from rGO to G/HA-80; however a sharp decrease is only observed from rGO to G/HA-20, and from G/HA-50 to G/HA-80. (**b**) Linear relationship between current and voltage measured using a potentiostat and two electrodes positioned at the top and bottom shell of the samples (inset). Only three samples are plotted because the curves of G/HA-20, -30, and -40 are similar.

Figure S8

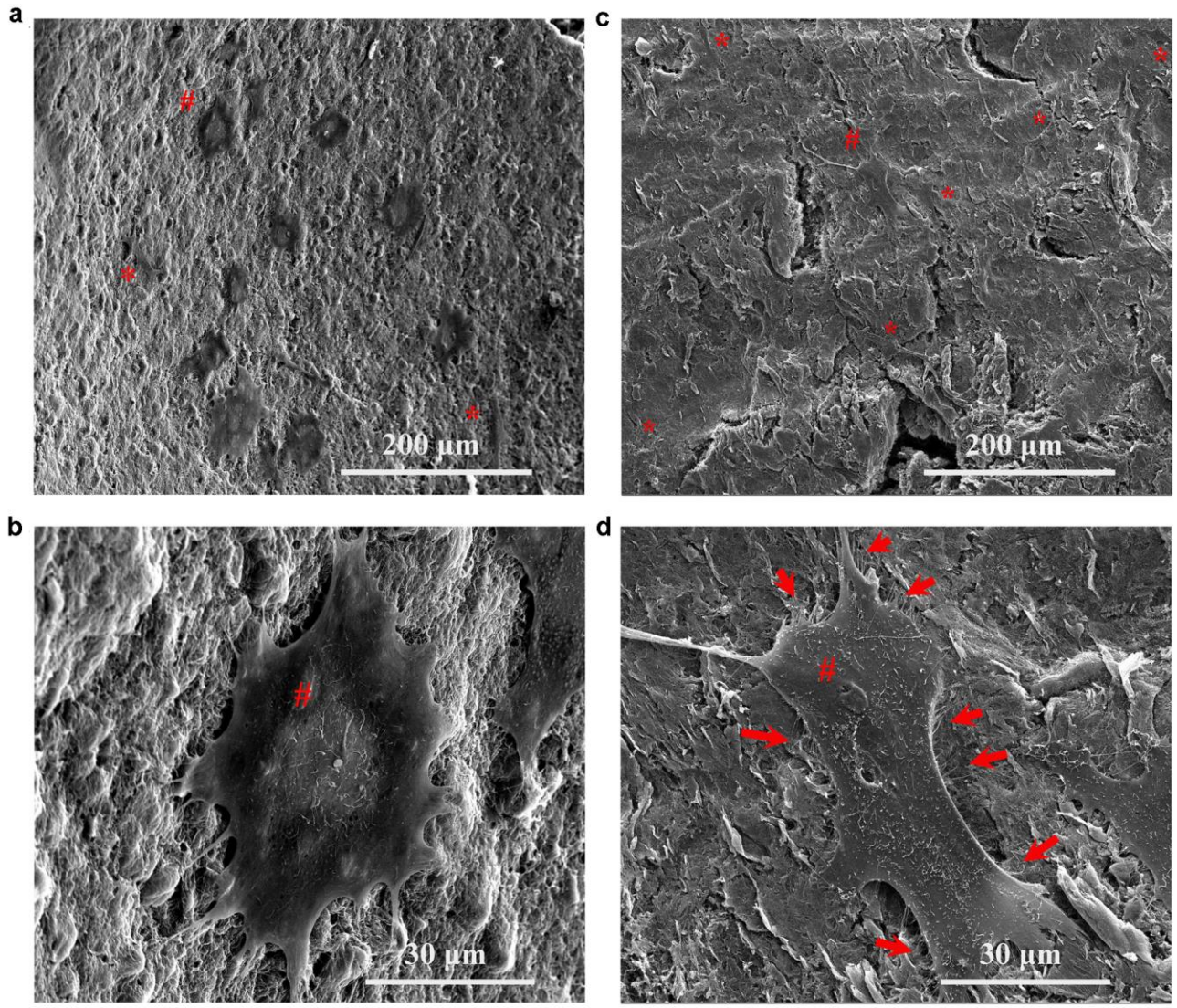

Figure S8. Cell morphology on rGO (a, b) and G/HA-40 (c, d).
(**a**) Most cells on rGO are roughly round, and only a few cells are well elongated (* labels). (**b**) The # labeled cell shows well spread morphology on rGO. (**c**) Almost all cells (# and * labels) on G/HA-40 are elongated and tightly adherent to the surface, making them hard to distinguish from the material surface. (**d**) The # labeled cell on G/HA-40 displays a high degree of elongation, with fine filamentous extensions (red arrows) linked to the material surface.

Supplementary Tables

Table S1. Elemental compositions of GO, rGO and G/HA-40 from XPS (*n*=3)

Sample	Composition (At %)							Ca/P	C/O
	C	O	N	Ca	P	Na	S		
GO [a]	30.0	68.4	0.85				0.76		2.28
	±0.2	±0.2	±0.02				±0.02		±0.02
rGO	85.13	10.08	4.17			0.62			8.44
	±0.06	±0.08	±0.06			±0.02			±0.07
G/HA-40	60.5	23.3	3.4	7.5	5.1	0.25		1.46	2.60
	±0.5	±0.3	±0.2	±0.4	±0.2	±0.01		±0.02	±0.03

[a] N and S elements were from traces of HNO_3 and H_2SO_4 used to prepare GO.

Table S2. Elemental composition of G/HA-40 from XPS spectra measured in various locations as schematized in Fig. 4a (main text).

Sampling Position	Etching level	Depth [a] (nm)	Composition (At %)					Ca/P	C/O
			C	O	N	Ca	P		
Bulk									
Section C			59 ±1	25±1	3.3±0.9	7.5±0.3	5.9±0.6	1.3±0.1	2.4±0.1
Section B			58±1	26±1	3.70±0.08	7.1±0.2	5.1±0.2	1.40±0.07	2.2±0.1
Section A			61±2	22.7±0.3	4±2	7.0±0.1	5.6±0.3	1.25±0.07	2.67±0.07
Shell									
Surface G									
Point 1 [b]	0	0	76.47	15.87	4.67	1.85	1.14	1.62	4.82
	1	1.4	81.51	9.93	3.91	2.97	1.68	1.77	8.21
	2	2.8	77.96	9.87	5.86	3.60	2.73	1.32	7.90
	3	6.8	80.62	9.79	3.81	3.41	2.37	1.44	8.23
Point 2	0	0	77.10	12.15	5.68	3.02	2.05	1.47	6.35
	1	14.4	77.66	10.78	5.07	3.90	2.58	1.51	7.20
	2	28.8	77.14	11.01	4.29	4.82	2.73	1.77	7.01
	3	43.2	76.75	11.97	3.57	4.66	3.05	1.53	6.41
Point 3	0	0	73.37	13.91	3.69	5.31	3.38	1.57	5.30
	1	14.4	73.90	13.41	3.25	6.04	3.39	1.78	5.51
	2	28.8	72.89	13.99	3.17	6.44	3.52	1.83	5.21
	3	43.2	70.5	14.42	4.87	6.68	3.53	1.89	4.89
Surface F									
Point 1	0	0	73.70	15.36	8.64	1.22	1.07	1.14	4.80
	1	14.4	82.72	8.85	5.70	1.81	0.93	1.94	9.35
	2	28.8	84.24	7.51	5.10	2.26	0.89	2.54	11.22
	3	43.2	83.51	7.95	5.71	2.19	0.63	3.48	10.50
Point 2	0	0	81.87	9.85	4.48	2.61	1.19	2.19	8.31
	1	14.4	82.72	8.50	4.81	2.95	1.02	2.89	9.73
	2	28.8	81.28	9.68	4.83	2.79	1.42	1.96	8.40
	3	43.2	81.60	8.56	5.56	3.01	1.27	2.37	9.53
Point 3	0	0	78.79	9.70	8.71	1.96	0.84	2.33	8.12
	1	14.4	82.29	7.09	6.90	2.62	1.10	2.38	11.61
	2	28.8	84.26	5.89	6.02	2.66	1.17	2.27	14.31
	3	43.2	83.41	6.59	6.19	2.90	0.91	3.19	12.66
Surface E									
Point 1	0	0	73.59	15.47	6.15	2.76	2.03	1.36	4.76
Point 2	0	0	74.30	15.68	5.71	2.50	1.80	1.39	4.74
Point 3	0	0	75.29	14.98	5.64	2.24	1.85	1.21	5.03
	1	14.4	79.36	10.49	3.94	3.62	2.58	1.40	7.57
	2	28.8	78.80	10.58	3.54	4.32	2.76	1.57	7.45

[a] The nominal depth on Ta_2O_5 at the same etching condition.

[b] The energy of etching Ar ion beam used on this point was lower than other points (3000 eV), i.e., 500 eV for etching level 1 and 2, and 1000 eV for level 3. Thus the Ca and P content increased more slowly.

References

1. Xu, Y. X.; Sheng, K. X.; Li, C.; Shi, G. Q. Self-assembled Graphene Hydrogel *via* a One-step Hydrothermal Process. *ACS Nano* **2010**, *4*, 4324–4330.
2. Gao, J.; Liu, F.; Liu, Y. L.; Ma, N.; Wang, Z. Q.; Zhang, X. Environment-friendly Method to Produce Graphene That Employs Vitamin C and Amino Acid. *Chem. Mater.* **2010**, *22*, 2213–2218.
3. Khalili, S.; Liu, Y. N.; Kornete, M.; Roescher, N.; Kodama, S.; Peterson, A.; Piccirillo, C. A.; Tran, S. D. Mesenchymal Stromal Cells Improve Salivary Function and Reduce Lymphocytic Infiltrates in Mice with Sjögren's-like Disease. *PLoS ONE* **2012**, *7*, e38615.
4. Jenkins, R.; Gould, R. W.; Gedcke, D. *Quantitative X-Ray Spectrometry* (2nd Edition); Marcel Decker Inc.: New York, 1995.